

# Deep Unfolding Convolutional Dictionary Model for Multi-Contrast MRI Super-resolution and Reconstruction

Pengcheng Lei<sup>1</sup>, Faming Fang<sup>1</sup>, Guixu Zhang<sup>1\*</sup> and Ming Xu<sup>2\*</sup>

<sup>1</sup>School of Computer Science and Technology, East China Normal University

<sup>2</sup>Software Engineering Institute, East China Normal University

pengchenglei1995@163.com, {fmfang, gxzhang, mxu}@cs.ecnu.edu.cn

## Abstract

Magnetic resonance imaging (MRI) tasks often involve multiple contrasts. Recently, numerous deep learning-based multi-contrast MRI super-resolution (SR) and reconstruction methods have been proposed to explore the complementary information from the multi-contrast images. However, these methods either construct parameter-sharing networks or manually design fusion rules, failing to accurately model the correlations between multi-contrast images and lacking certain interpretations. In this paper, we propose a multi-contrast convolutional dictionary (MC-CDic) model under the guidance of the optimization algorithm with a well-designed data fidelity term. Specifically, we built an observation model for the multi-contrast MR images to explicitly model the multi-contrast images as common features and unique features. In this way, only the useful information in the reference image can be transferred to the target image, while the inconsistent information will be ignored. We employ the proximal gradient algorithm to optimize the model and unroll the iterative steps into a deep CDic model. Especially, the proximal operators are replaced by learnable ResNet. In addition, multi-scale dictionaries are introduced to further improve the model performance. We test our MC-CDic model on multi-contrast MRI SR and reconstruction tasks. Experimental results demonstrate the superior performance of the proposed MC-CDic model against existing SOTA methods. Code is available at <https://github.com/lpcccc-cv/MC-CDic>.

## 1 Introduction

Magnetic Resonance Imaging (MRI) is a noninvasive and non-ionizing medical imaging technique widely used for medical diagnosis, clinical analysis, and staging of disease [Song *et al.*, 2019a]. However, due to the physics and physiological constraints, the MRI scanning procedure is always time-consuming. The scanning time of each patient can

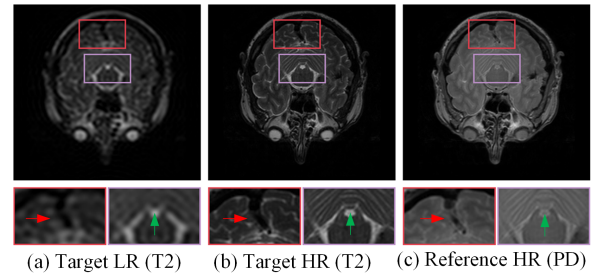


Figure 1: The visual comparison of the multi-contrast images, i.e. T2 and PD, on IXI dataset. They share some common textures (in green), and they also have their unique contrast information and some inconsistent structures (in red).

take up to ten minutes long, which seriously affects the patient experience and leads to high costs [Feng *et al.*, 2022]. To accelerate the MRI procedure, a commonly used approach is to undersample the k-space measurements and then use the reconstruction algorithm to restore its fully sampled imaging. The recent mainstream methods for accelerating MRI include MRI reconstruction and MRI super-resolution (SR). MRI reconstruction aims to remove the aliasing artifacts caused by k-space undersampling. MRI SR aims to reconstruct high-resolution (HR) MR images from low-resolution (LR) images. Both two methods can effectively improve the quality of MR images and accelerate MRI without upgrading hardware facilities.

In the past few years, numerous MRI SR [Zhao *et al.*, 2019; Wang *et al.*, 2021; Zhang *et al.*, 2021b] and reconstruction [Wang *et al.*, 2016; Zheng *et al.*, 2019; Nitski *et al.*, 2020] methods have been proposed. However, they only use single-contrast MR images, ignoring complementary information from multi-contrast images. In clinical practice, scanners usually produce exquisite images of body parts with different contrasts, such as T1-weighted, T2-weighted, and proton density weighted images (PD). These contrasts capture the information with the same underlying anatomy and thus exhibit similar structures [Lyu *et al.*, 2020]. Furthermore, since the repetition time and echo time of different contrasts are different. For example, the scanning time of T1 and PD are significantly shorter than those of T2, so it is promising to leverage an HR (or fully sampled) reference image with a shorter acquisition time to reconstruct the modality with a

\*Corresponding author

longer scanning time from an LR (or undersampled) image. We name them guided-SR and guided-reconstruction.

Recently, deep convolutional neural network (DCNN) [Liu and Lei, 2021] has become a mainstream approach for solving MRI guided-SR problems. [Lyu *et al.*, 2020] proposed to fuse the multi-contrast information in the high-level feature space. [Feng *et al.*, 2021] used a multi-stage integration network to explore the rich relations among different contrasts. [Li *et al.*, 2022; Fang *et al.*, 2022] designed a transformer-based framework to fully explore the long-range dependencies in both reference and target images. For solving the multi-contrast reconstruction problem, [Xiang *et al.*, 2018] fused multi-contrast MR acquisitions through deep networks to speed up the reconstruction of a certain target image. [Sun *et al.*, 2019] proposed a deep information-sharing network to jointly reconstruct multi-contrast MRI images. [Dar *et al.*, 2020] employed an auxiliary contrast as prior information into the generator of a generative adversarial network (GAN) to accelerate MR imaging. [Zhang *et al.*, 2021a] applied the temporal feature fusion block based on ADMM to achieve multi-modal MRI reconstruction. [Feng *et al.*, 2022] proposed a multi-modal transformer (MTrans) to transfer multi-scale features from the target modality to the auxiliary one.

Although these methods have gotten promising results, their network architectures are black-boxes, making it difficult to understand the underlying mechanism and lack certain physical interpretations. As is well known, the model-based method [Song *et al.*, 2019b] is explainable and easy to incorporate domain knowledge. Most recently, numerous well-designed model-driven DCNN methods have been proposed to solve various image restoration problems, including deraining [Wang *et al.*, 2020], deblurring [Liu *et al.*, 2019], image fusion [Liu *et al.*, 2021] and so on. For MR images, [Yang *et al.*, 2018; Aggarwal *et al.*, 2018; Sriram *et al.*, 2020] proposed model-based reconstruction methods based on the compressed sensing theory. However, they are designed for single-contrast MRI reconstruction.

In this paper, we propose a novel multi-contrast convolutional dictionary (MC-CDic) model to explicitly model the correlations of multi-contrast images for guided-SR and reconstruction tasks. MC-CDic model is designed by the following two observations. First, the multi-contrast images are sampled under the same anatomical structure, they thus share some common features, e.g., edges and texture information. Second, since the two images are generated by different scan settings, they also have their unique contrast information and some unaligned inconsistent structures, as shown in Figure 1. *To better reconstruct the target image, we hope to transfer the common texture information from the reference image to the target image while avoiding the interference of inconsistent information.* Taking these into consideration, we first extract the common features and unique features from the multi-contrast images and then fuse these features to generate the desired high-quality images.

To extract the features from both images, firstly, we adopt the convolutional sparse coding (CSC) technique to model the multi-contrast MR images. Specifically, the multi-contrast images are decomposed into two types of features (i.e., common features and unique features) using two types of dictio-

naries (i.e., common filters and unique filters). Secondly, we employ implicit regularizations on the decomposed features and use the proximal gradient algorithm to optimize them. Thirdly, we unfold the iterative optimization process into a deep network. Especially, the unfolding process strictly follows the rules of the solution and the proximal operators are replaced by learnable residual blocks. Thus all the parameters can be learned in an end-to-end manner. Fourthly, we further employ multi-scale dictionaries to extract the multi-scale sparse representations in each iteration. In this way, the proposed network is not only interpretable but also powerful. Our contributions can be summarized as follows.

- We propose a deep unfolding network based on convolutional dictionary learning for multi-contrast MRI SR and reconstruction. Different from existing methods that design unsophisticated fusion rules, we develop priors and constraints plugged into the model according to the characteristics of multi-contrast MR images.
- We build an observation model for multi-contrast MRI using the CSC technique and use the proximal gradient algorithm to solve the model. Based on the iterative solutions, we unroll the iteration steps into a multi-scale convolutional dictionary network and the proximal operators are replaced by learnable deep residual networks.
- The proposed model combines the good interpretability of the dictionary model with powerful deep neural networks. We test it on guided MRI SR and reconstruction tasks. Extensive experiments on the benchmark datasets demonstrate the effectiveness of the proposed model.

## 2 MC-CDic Model for MR Images

### 2.1 Model Formulation

Let  $\hat{x}_1 \in \mathbb{R}^{m \times n}$  and  $\hat{x}_2 \in \mathbb{R}^{m \times n}$  denote two classes of HR (or fully-sampled) MR images with different contrasts (e.g. PD and T2). The corresponding LR (or undersampled) images of  $\hat{x}_2$  is  $x_2$ . For the guided-SR task, our MC-CDic model aims to restore the HR image  $\hat{x}_2$  from LR image  $x_2$  with the aid of the reference HR image  $\hat{x}_1$ . Since the two contrast images are sampled under the same anatomical structure, they share some common features. Since they are sampled under different scan setting, they also have their unique features. Based on these observations, inspired by [Deng and Dragotti, 2020], we model the multi-contrast images as:

$$\hat{x}_1 = \sum_k d_k^c \otimes c_k + \sum_k d_k^u \otimes u_k, \quad (1)$$

$$x_2 = \sum_k h_k^c \otimes c_k + \sum_k h_k^v \otimes v_k, \quad (2)$$

where  $\otimes$  denotes the convolutional operation.  $\{d_k^c\}_{k=1}^K$  and  $\{h_k^c\}_{k=1}^K$  are the common filters of  $\hat{x}_1$  and  $x_2$ ,  $\{d_k^u\}_{k=1}^K$  and  $\{h_k^v\}_{k=1}^K$  are the unique filters of  $\hat{x}_1$  and  $x_2$ ,  $\{c_k\}_{k=1}^K$  represent the common features between  $\hat{x}_1$  and  $x_2$ ,  $\{u_k\}_{k=1}^K$  and  $\{v_k\}_{k=1}^K$  represent the unique features of  $\hat{x}_1$  and  $x_2$ .  $K$  denotes the channel numbers of the feature representations.

Based on the decomposed common features and unique features, the reconstructed HR image can be represented as:

$$\hat{x}'_2 = \sum_k q_k^c \otimes c_k + \sum_k q_k^v \otimes v_k, \quad (3)$$

where  $\{q_k^c\}_{k=1}^K$  and  $\{q_k^v\}_{k=1}^K$  are the common filters and the unique filters for reconstructing the HR images  $\hat{x}'_2$ .

For the above modeling, the main problem is to extract the common features and the unique features from the input images. Assuming all the filters are known, they can be solved by optimizing the following problem:

$$\begin{aligned} \min_{\{C,U,V\}} \frac{1}{2} \|\hat{x}_1 - \sum_k (d_k^c \otimes c_k + d_k^u \otimes u_k)\|_F^2 \\ + \frac{1}{2} \|x_2 - \sum_k (h_k^c \otimes c_k + h_k^v \otimes v_k)\|_F^2 \\ + \lambda_c \psi_c(C) + \lambda_u \psi_u(U) + \lambda_v \psi_v(V), \end{aligned} \quad (4)$$

where  $\{C, U, V\} \in \mathbb{R}^{m \times n \times K}$  are the stacked features response to  $\{c, u, v\}_{k=1}^K$ ,  $\lambda_c, \lambda_u, \lambda_v$  are the trade-off parameters,  $\psi_c(\cdot), \psi_u(\cdot), \psi_v(\cdot)$  are the regularizers to deliver the prior information to the feature maps.

## 2.2 Optimization Algorithm

To solve this problem, we alternately update each variable with other variables fixed. It leads to the following three sub-problems:

$$\min_U \frac{1}{2} \|\hat{x}_1 - \sum_k (d_k^c \otimes c_k + d_k^u \otimes u_k)\|_F^2 + \lambda_u \psi_u(U), \quad (5)$$

$$\min_V \frac{1}{2} \|x_2 - \sum_k (h_k^c \otimes c_k + h_k^v \otimes v_k)\|_F^2 + \lambda_v \psi_v(V), \quad (6)$$

$$\begin{aligned} \min_C \frac{1}{2} \|\hat{x}_1 - \sum_k (d_k^c \otimes c_k + d_k^u \otimes u_k)\|_F^2 \\ + \frac{1}{2} \|x_2 - \sum_k (h_k^c \otimes c_k + h_k^v \otimes v_k)\|_F^2 + \lambda_c \psi_c(C). \end{aligned} \quad (7)$$

Next, we optimize these three subproblems separately using the proximal gradient method. The details are as follows:

**Updating  $U$ .** The unique feature of  $\hat{x}_1, U$  can be updated by solving the quadratic approximation [Beck and Teboulle, 2009] of the subproblem (5) as:

$$\min_U \frac{1}{2} \|U - (U^{t-1} - \eta_u \nabla f(U^{t-1}))\|_F^2 + \eta_u \lambda_u \psi_u(U), \quad (8)$$

where  $U^{t-1}$  is the updating result of the last iteration,  $\eta_u$  is the stepsize parameter, and

$$f(U^{t-1}) = \frac{1}{2} \|\hat{x}_1 - \sum_k (d_k^c \otimes c_k^{t-1} + d_k^u \otimes u_k^{t-1})\|_F^2, \quad (9)$$

$$\nabla f(U^{t-1}) = D^u \otimes^\top \left( \sum_k (d_k^c \otimes c_k^{t-1} + d_k^u \otimes u_k^{t-1}) - \hat{x}_1 \right), \quad (10)$$

where  $\otimes^\top$  denotes the transposed convolution,  $D^u \in \mathbb{R}^{1 \times n \times n \times K}$  is a 4-D tensor stacked by  $\{d_k^u\}_{k=1}^K$ . Eq. (10) can be re-written as:

$$\nabla f(U^{t-1}) = D^u \otimes^\top (D^c \otimes C^{t-1} + D^u \otimes U^{t-1}) - D^u \otimes^\top \hat{x}_1, \quad (11)$$

where  $D^c \in \mathbb{R}^{1 \times n \times n \times K}$  is a 4-D tensor stacked by  $\{d_k^c\}_{k=1}^K$ . Corresponding to general regularization term [Donoho, 1995], the solution of Eq. (8) is:

$$U^t = \text{prox}_{\eta_u \lambda_u} (U^{t-1} - \eta_u \nabla f(U^{t-1})), \quad (12)$$

where  $\text{prox}_{\eta_u \lambda_u}(\cdot)$  is the proximal operator dependent on the regularization term  $\psi_u(\cdot)$  with respect to  $U$ . Instead of choosing a fixed regularizer in the model, the form of the proximal operator can be automatically learned from training data.

**Updating  $V$ .** Similarly, the quadratic approximation of the problem (6) with respect to  $V$  is:

$$\min_V \frac{1}{2} \|V - (V^{t-1} - \eta_v \nabla f(V^{t-1}))\|_F^2 + \eta_v \lambda_v \psi_v(V) \quad (13)$$

where

$$f(V^{t-1}) = \frac{1}{2} \|x_2 - \sum_k (h_k^c \otimes c_k^{t-1} + h_k^v \otimes v_k^{t-1})\|_F^2, \quad (14)$$

$$\nabla f(V^{t-1}) = H^v \otimes^\top \left( \sum_k (h_k^c \otimes c_k^{t-1} + h_k^v \otimes v_k^{t-1}) - x_2 \right). \quad (15)$$

$H^v \in \mathbb{R}^{1 \times n \times n \times K}$  is a 4-D tensor stacked by  $\{h_k^v\}_{k=1}^K$ . Eq. 15 can be re-written as:

$$\nabla f(V^{t-1}) = H^v \otimes^\top (H^c \otimes C^{t-1} + H^v \otimes V^{t-1}) - H^v \otimes^\top x_2, \quad (16)$$

where  $H^c \in \mathbb{R}^{1 \times n \times n \times K}$  is a 4-D tensor stacked by  $\{h_k^c\}_{k=1}^K$ . The solution of Eq. (13) can be represented as:

$$V^t = \text{prox}_{\eta_v \lambda_v} (V^{t-1} - \eta_v \nabla f(V^{t-1})), \quad (17)$$

where  $\text{prox}_{\eta_v \lambda_v}(\cdot)$  is the proximal operator correlated to the regularization term  $\psi_v(\cdot)$  with respect to  $V$ .

**Updating  $C$ .** We first denote  $\tilde{x}_1 = \hat{x}_1 - \sum_k d_k^u \otimes u_k$  and  $\tilde{x}_2 = x_2 - \sum_k h_k^v \otimes v_k$ , Eq. (7) can be re-written as follows:

$$\min_C \frac{1}{2} \|\tilde{x}_1 - \sum_k d_k^c \otimes c_k\|_F^2 + \frac{1}{2} \|\tilde{x}_2 - \sum_k h_k^c \otimes c_k\|_F^2 + \lambda_c \psi_c(C) \quad (18)$$

Then the first two terms in Eq. (18) can be further combined and this yields the following optimization problem:

$$\min_C \frac{1}{2} \|M - \sum_k l_k^c \otimes c_k\|_F^2 + \lambda_c \psi_c(C) \quad (19)$$

where  $M$  is the concatenate of  $\tilde{x}_1$  and  $\tilde{x}_2$ ,  $l_k^c$  is the concatenate of  $d_k^c$  and  $h_k^c$ . Thus, Eq. (19) can be solved by the same way as  $U$  and  $V$ . Specifically, the quadratic approximation of this problem to  $C$  is:

$$\min_C \frac{1}{2} \|C - (C^{t-1} - \eta_c \nabla f(C^{t-1}))\|_F^2 + \eta_c \lambda_c \psi_c(C) \quad (20)$$

where

$$f(C^{t-1}) = \frac{1}{2} \|M - \sum_k l_k^c \otimes c_k^{t-1}\|_F^2, \quad (21)$$

$$\nabla f(C^{t-1}) = L^c \otimes^\top \sum_k (l_k^c \otimes c_k^{t-1} - M), \quad (22)$$

where  $L^c \in \mathbb{R}^{n \times n \times K \times 2}$  is a 4-D tensor stacked by  $\{l_k^c\}_{k=1}^K$ . Eq. (22) can be re-written as:

$$\nabla f(C^{t-1}) = L^c \otimes^\top (L^c \otimes C^{t-1}) - L^c \otimes^\top M, \quad (23)$$

The solution of Eq.(20) can be represented as:

$$C^t = \text{prox}_{\eta_c \lambda_c} (C^{t-1} - \eta_c \nabla f(C^{t-1})), \quad (24)$$

where  $\text{prox}_{\eta_c \lambda_c}(\cdot)$  is the proximal operator correlated to the regularization term  $\psi_c(\cdot)$  with respect to  $C$ .

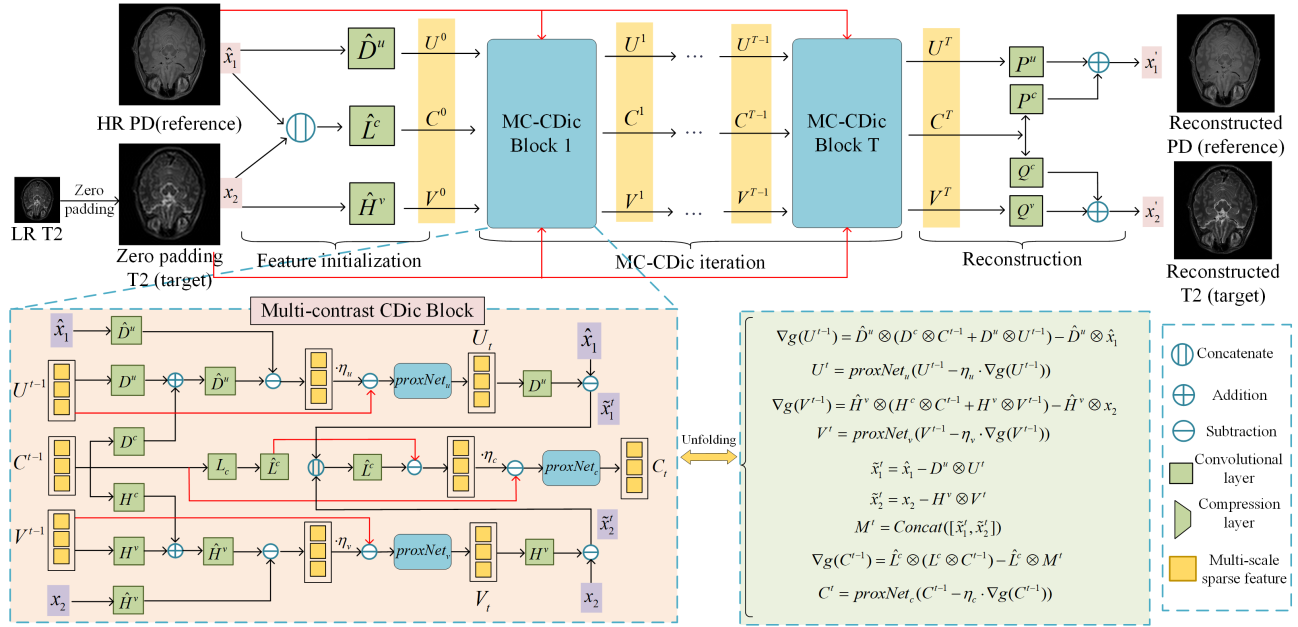


Figure 2: The overall structure of the proposed multi-contrast convolutional dictionary (MC-CDic) model for the guided-SR task.

### 3 Deep Unfolding MC-CDic Model

Before unfolding the above model, we first formulate some relaxations on the dictionaries. Following earlier works [Simon and Elad, 2019; Lecouat *et al.*, 2020b; Lecouat *et al.*, 2020a; Liu *et al.*, 2022], we untie the convolutional dictionaries from their transposed convolutional dictionaries in Eq. (11), (16) and (23) for better performance. To be specific, we initialize the convolution dictionary  $D^u \otimes$  identically to  $D^u \otimes^\top$  but are allowed to evolve independently during training. For convenience, we use  $\hat{D}^u \otimes$  to replace  $D^u \otimes^\top$ . Similarly,  $H^v \otimes^\top$  and  $L^c \otimes^\top$  are also replaced by  $\hat{H}^v \otimes$  and  $\hat{L}^c \otimes$  in our deep unfolding model.

#### 3.1 Network Design

**(1) Feature Initialization Module.** We use three convolutional dictionaries to initialize the common features and the unique features from the multi-contrast images  $\hat{x}_1$  and  $x_2$ . Specifically, we first use the dictionaries  $\hat{D}^u$  and  $\hat{H}^v$  to initialize the unique feature  $U^0$  and  $V^0$  respectively. Then we concatenate  $\hat{x}_1$  and  $x_2$ , and use  $\hat{L}^c$  to initialize the common feature  $C^0$ .

**(2) MC-CDic Iteration Module.** As shown in the figure, our model consists  $T$  MC-CDic blocks, representing  $T$  iterations of the algorithm for solving Eq. (4). Specifically, we take the input images  $\hat{x}_1$  and  $x_2$ , and the previous outputs  $U^{t-1}$ ,  $V^t$  and  $C^t$  as inputs, and outputs the updated  $U^{t+1}$ ,  $V^{t+1}$  and  $C^{t+1}$  in each iteration block. The iteration blocks are unfolded following the updating rules of Eq. (12), (17) and (24). To be specific, the convolutional dictionary operations can be easily implemented by the commonly used convolutional layers in normal networks. The key issue of unrolling the algorithm is how to represent the three proximal operators  $\text{prox}_{\eta_u \lambda_u}(\cdot)$ ,  $\text{prox}_{\eta_v \lambda_v}(\cdot)$  and  $\text{prox}_{\eta_c \lambda_c}(\cdot)$ . In-

spired by recent unfolding networks [Wang *et al.*, 2020; Wang *et al.*, 2022], we employ the deep residual network (ResNet) to replace the proximal operators. Note that the  $T$  MC-CDic iterations share the same parameters in our model.

Thus, at the  $t^{\text{th}}$  stage, the network for updating  $U$  can be built as:

$$\begin{cases} \nabla f(U^{t-1}) = \hat{D}^u \otimes (D^c \otimes C^{t-1} + D^u \otimes U^{t-1}) - \hat{D}^u \otimes \hat{x}_1, \\ U^t = \text{proxNet}_u(U^{t-1} - \eta_u \nabla f(U^{t-1})), \end{cases} \quad (25)$$

where  $\text{proxNet}_u(\cdot)$  denotes the ResNet with several res-blocks. Similarly, the network for updating  $V$  at the  $t^{\text{th}}$  stage can be built as:

$$\begin{cases} \nabla f(V^{t-1}) = \hat{H}^v \otimes (H^c \otimes C^{t-1} + H^v \otimes V^{t-1}) - \hat{H}^v \otimes x_2, \\ V^t = \text{proxNet}_v(V^{t-1} - \eta_v \nabla f(V^{t-1})), \end{cases} \quad (26)$$

where  $\text{proxNet}_v(\cdot)$  denotes the ResNet with several res-blocks.

Based on the updated unique features  $U^t$  and  $V^t$ , the network for updating  $C$  at the  $t^{\text{th}}$  stage can be built as:

$$\begin{cases} \bar{x}_1^t = x_1 - D^u \otimes U^t, \\ \bar{x}_2^t = x_2 - H^v \otimes V^t, \\ M^t = \text{Concat}([\bar{x}_1^t, \bar{x}_2^t]), \\ \nabla f(C^{t-1}) = \hat{L}^c \otimes (L^c \otimes C^{t-1}) - \hat{L}^c \otimes M^t, \\ C^t = \text{proxNet}_c(C^{t-1} - \eta_c \nabla f(C^{t-1})), \end{cases} \quad (27)$$

where  $\text{proxNet}_c(\cdot)$  denotes the ResNet with several res-blocks,  $M^t$  is the concatenated features of  $\bar{x}_1^t$  and  $\bar{x}_2^t$ . According to the updating rules of  $U$ ,  $V$  and  $C$  in Eq. (25), (26) and (27), we design the multi-contrast convolutional dictionary (MC-CDic) block. Its overall structure is shown in Figure 2. All the parameters involved can be automatically learned from training data in an end-to-end manner.

**(3) Reconstruction Module.** After  $T$  MC-CDic iterations, we get the final common features  $C^T$  and the final unique

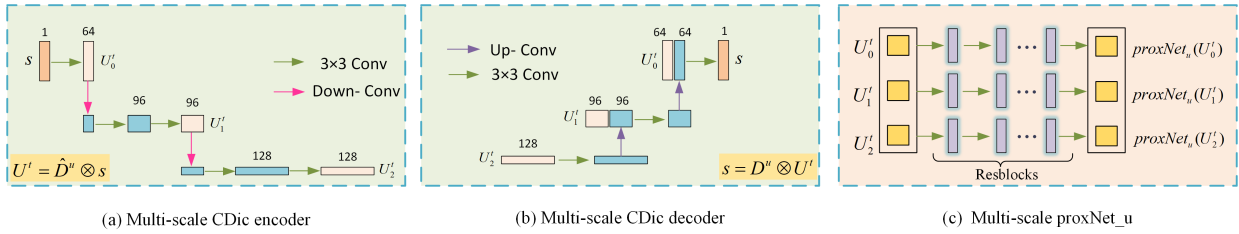


Figure 3: The structure of the proposed multi-scale dictionaries (for updating  $U^t$ ). (a) multi-scale CDic encoder, (b) multi-scale CDic decoder, and (c) multi-scale proximal network.  $U_t = \{U_0^t, U_1^t, U_2^t\}$  contains a list of multi-scale representations.

feature  $U^T$  and  $V^T$ . Then the reconstructed HR image  $x'_2$  can be obtained by:

$$x'_2 = Q^c \otimes C^T + Q^u \otimes V^T, \quad (28)$$

where  $Q^c = \{q_k^c\}_{k=1}^K$  and  $Q^u = \{q_k^u\}_{k=1}^K$  are the common filters and unique filters for reconstructing the HR images.

### 3.2 Multi-Scale Dictionaries

The importance of multi-scale representations has been proven in numerous computer vision tasks. However, most existing CDic models only use the single-scale dictionary to extract single-scale representations, which limits their performance to a large extent. Inspired by [Liu *et al.*, 2022], we employ the multi-scale dictionaries in our MC-CDic model to perceive the multi-scale representations. To be specific, we employ a stripped-down version of the image synthesis process of U-Net by removing all non-linearities, batch normalization, and additive biases. We regard the decoder part of the UNet as a normal CDic layer and regard the encoder part of the UNet as its transposed CDic layer. As shown in Figure 3 (a) and (b), we present the operations of  $U^t = \hat{D}^u \otimes s$  and  $s = D^u \otimes U^t$ . The proximal network for multi-scale dictionaries is shown in Figure 3 (c).

### 3.3 Loss Function

We employ the simple L1 loss to supervise the multi-contrast images simultaneously. It can be formulated as:

$$\mathcal{L} = \alpha \|x'_1 - \hat{x}_1\|_1 + \|x'_2 - \hat{x}_2\|_1, \quad (29)$$

where  $\alpha$  is a trade-off parameter to balance the importance of different contrasts. In this paper, we set  $\alpha = 0.1$ . Note that the loss on the reference image is to ensure that the reference image can be efficiently decomposed.

## 4 Experiments

### 4.1 Datasets

Following [Lyu *et al.*, 2020; Fang *et al.*, 2022], we employ two publicly available multi-modal MR image datasets, IXI and BraTS2018 [Menze *et al.*, 2015] to validate the effectiveness of our model. IXI dataset contains 576 multi-contrast MR volumes and we employ the PD as the reference modal to guide the reconstruction of the target T2 modal. The BraTS2018 dataset contains 285 multi-contrast MR volumes and we employ the T1 as the reference modality to guide the reconstruction of the target T2 modal. We split

Method	Params	IXI-T2			BrainTS-T2		
		PSNR $\uparrow$	SSIM $\uparrow$	RMSE $\downarrow$	PSNR $\uparrow$	SSIM $\uparrow$	RMSE $\downarrow$
ZP	-	30.43	0.8840	8.15	32.40	0.8873	6.38
VDSR	0.7M	32.51	0.9162	6.37	35.53	0.9580	4.46
CSN	11.2M	34.04	0.9365	5.35	36.30	0.9633	4.08
RCAN	15.6M	34.44	0.9413	5.12	36.81	0.9670	3.84
SwinIR	11.9M	34.37	0.9402	5.17	36.99	0.9680	3.77
CUNet	0.2M	39.65	0.9720	2.77	38.17	0.9710	3.32
MCSR	3.5M	40.00	0.9734	2.67	38.09	0.9718	3.36
MASA	4.0M	41.45	0.9786	2.23	37.66	0.9700	3.50
MCMRSR	3.5M	40.93	0.9753	2.53	37.82	0.9660	3.45
MINet	11.9M	41.70	0.9784	2.22	39.46	0.9758	2.88
Ours-S	1.9M	41.96	0.9792	2.16	39.87	0.9773	2.76
Ours-L	9.6M	<b>42.58</b>	<b>0.9810</b>	<b>2.01</b>	<b>40.75</b>	<b>0.9806</b>	<b>2.49</b>

Table 1: Quantitative results of single-contrast MRI SR and multi-contrast MRI guided-SR algorithms when scaling factor is  $\times 4$ .

the two datasets patient-wisely into a ratio of 7:1:2 for training/validation/testing. For each volume, we only select the middle 100 slices for our experiments. We use the cartesian sampling mask and the k-space center cropping [Lyu *et al.*, 2020] mask to get the undersampled and LR images, respectively. The acceleration ratio for reconstruction and the scale factor for SR are set at 4.

### 4.2 Implementation Details

**Training Details.** Our proposed MC-CDic model is implemented in PyTorch with an NVIDIA RTX3090 GPU. We adopt the Adam optimizer with a batch size of 6. The learning rate is set to  $1 \times 10^{-4}$  and the models are trained 50 epochs. We employ the peak-to-noise-ratio (PSNR), structural similarity index (SSIM), and root mean squared error (RMSE) to evaluate the model performance. The higher the PSNR and SSIM, the lower the RMSE represents the better result.

**Model Details.** In our large model MC-CDic-L, the iteration stage  $T$  is set to 4. The levels of the multi-scale dictionaries are set to 3. From the first level to the third level, the channel numbers of the features are set to 64, 96, and 128. The numbers of the resblocks for the multi-scale proximal network are set to 5, 3, and 1. In our small model MC-CDic-S, we use the single-scale dictionary and other settings are the same with MC-CDic-L.

### 4.3 Comparison with State-of-the-arts

**Evaluations on Guided-SR.** Guided-SR aims to reconstruct the HR image from its LR image with the aid of an-

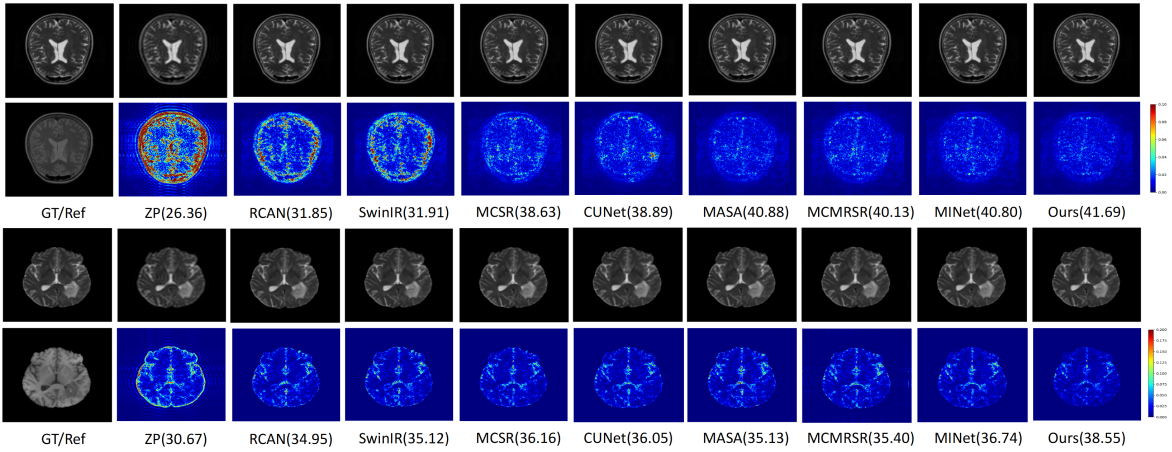


Figure 4: Error maps of different single-contrast SR (the first three methods) and guided-SR (the next six methods) with the scale factor of  $\times 4$  on the IXI (PD guides T2) and BrainTS (T1 guides T2) testing sets.

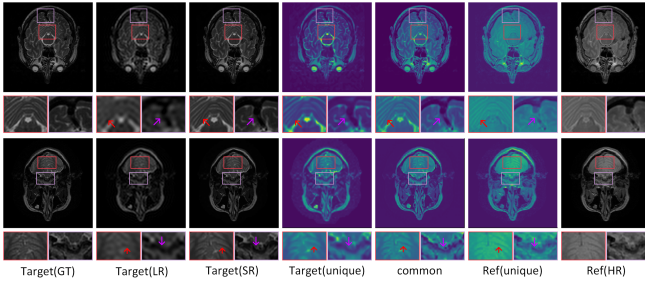


Figure 5: Visualization of the decomposed common and unique components of our MC-CDic model on the guided-SR task.

other reference HR image. We compare our methods with various single image SR approaches, including VDSR [Kim *et al.*, 2016], CSN [Zhao *et al.*, 2019], RCAN [Zhang *et al.*, 2018] and SwinIR [Liang *et al.*, 2021], and various multi-contrast guided-SR methods, including MCSR [Lyu *et al.*, 2020], CUNet [Deng and Dragotti, 2020], MASA [Lu *et al.*, 2021], MINet [Feng *et al.*, 2021] and MCMRSR [Li *et al.*, 2022]. The quantitative results of these methods are shown in Table 1. Among these methods, our MC-CDic-L model gets the best performance. It outperforms MINet by 0.92dB and 1.29dB in PSNR on the IXI and BrainTS datasets, respectively. Our MC-CDic-S only has 1.9M parameters, but it outperforms most existing SOTA methods. We randomly select two images from the two test sets and visualize the error maps of different methods in Figure 4. As one can see, the results of our methods have fewer errors than other methods. In Figure 5, we visualize the decomposed components of our MC-CDic model on the guided-SR task. The common feature represents the learned complementary information from the reference HR image to the target LR image. By decomposing the multi-contrast images, our method can only focus on the details (red arrows) related to the target image and avoid the interference of inconsistent information (purple arrows).

**Evaluations on Guided Reconstruction.** Guided reconstruction aims to reconstruct a clear image from its under-sampled image with the aid of another auxiliary fully-

Method	Params	IXI-T2			BrainTS-T2		
		PSNR $\uparrow$	SSIM $\uparrow$	RMSE $\downarrow$	PSNR $\uparrow$	SSIM $\uparrow$	RMSE $\downarrow$
ZF	-	27.27	0.6188	11.69	28.72	0.6932	9.70
UNet	7.8M	33.24	0.9246	5.85	31.07	0.9443	7.83
MUSC	13.9M	34.39	0.9326	5.23	37.11	0.9644	3.71
Restormer	26.1M	35.79	0.9481	4.40	38.15	0.9699	3.31
CUNet	0.2M	37.30	0.9577	3.61	36.46	0.9629	4.04
MDUNet	5.2M	39.79	0.9715	2.75	35.26	0.9632	5.68
MTrans	86.1M	39.48	0.9700	2.96	34.02	0.9473	5.33
Restormer*	26.1M	<u>41.61</u>	<u>0.9780</u>	<u>2.24</u>	<u>39.91</u>	<u>0.9778</u>	<u>2.75</u>
Ours-S	1.9M	41.08	0.9765	2.37	39.75	0.9765	2.79
Ours-L	9.6M	<b>42.00</b>	<b>0.9802</b>	<b>2.14</b>	<b>41.65</b>	<b>0.9829</b>	<b>2.26</b>

Table 2: Quantitative results of single-contrast MRI reconstruction and multi-contrast guided-reconstruction algorithms at  $\times 4$  acceleration.

sampled image. Here we compare our MC-CDic model with single-contrast reconstruction methods, including zero filling (ZF), UNet [Ronneberger *et al.*, 2015], MUSC [Liu *et al.*, 2022] and Restormer [Zamir *et al.*, 2022], and multi-contrast guided-reconstruction methods, including MDUNet [Xiang *et al.*, 2018], MTrans [Feng *et al.*, 2022] and Restormer\* [Zamir *et al.*, 2022]. Note that Restormer\* employs multi-contrast images as input to restore the target contrast images. Quantitative results are shown in Table 2. From the table, we can find that our MC-CDic-L achieves the best performance on the two testing sets. Restormer\* outperforms our MC-CDic-S, but it has far more parameters than our model. Visual comparisons are shown in Figure 6, our method can restore more anatomical details than other methods. It fully demonstrates the superiority of our method.

#### 4.4 Ablation Analysis

**The Effect of the Number of Stages  $T$ .** To show how the number of iteration stages  $T$  affects the reconstruction performance, we have compared the proposed MC-CDic method with different stages. Figure 7 shows the average PSNR and SSIM performance for the guided-SR task and guided-reconstruction task on the IXI validation set when  $T \in [1, 5]$ . It can be observed that more stages lead to improved recon-

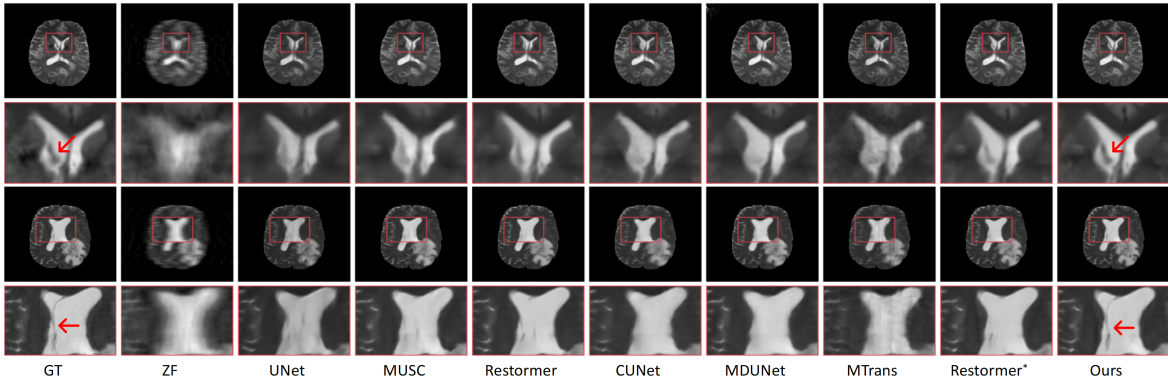


Figure 6: Visual comparison of different single-contrast reconstruction (the first four methods) and multi-contrast guided reconstruction (the last five methods) on the IXI (PD guides T2) and BrainTS (T1 guides T2) testing sets when acceleration is  $\times 4$ .

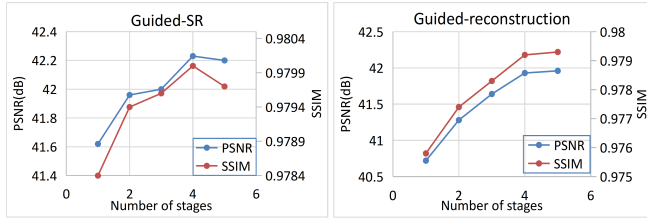


Figure 7: The PSNR and SSIM curves on IXI validation set with a different number of stages  $T$ .

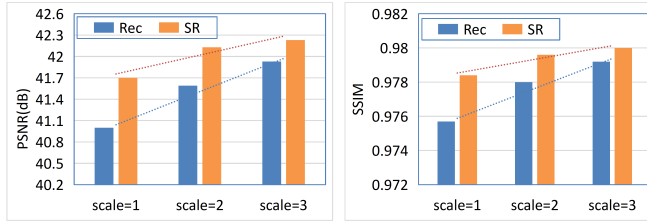


Figure 8: PSNR and SSIM comparisons on IXI dataset with different levels of multi-scale dictionaries.

struction performance. Specifically, from  $T = 1$  to  $T = 4$ , the psnr improves 0.6dB and 1.4dB in the guided-SR and guided-reconstruction tasks, respectively. To balance the performance and the computational complexity, we manually set  $T = 4$  in our final model.

**The Effect of the Multi-Scale Dictionaries.** We compare the performance of the proposed MC-CDic model under different levels of multi-scale dictionaries in Figure 8. From the figure, we can find that the performance increases with the feature levels. From the trend lines, we can also see that multi-scale features are more important for the reconstruction task. Specifically, three levels of feature improve the PSNR by about 0.5dB and 0.9dB compared with the single-level features on the SR and reconstruction tasks, respectively. More feature levels may achieve better performance, however, the number of parameters and computations will also increase. To balance the performance and the computational complexity, we set the feature level as 1 in our MC-CDic-S and set the

Method	Guided-SR			Guided-reconstruction		
	PSNR $\uparrow$	SSIM $\uparrow$	RMSE $\downarrow$	PSNR $\uparrow$	SSIM $\uparrow$	RMSE $\downarrow$
w/o proxNet	42.15	0.9799	2.11	40.94	0.9770	2.42
w proxNet	<b>42.58</b>	<b>0.9810</b>	<b>2.01</b>	<b>42.00</b>	<b>0.9802</b>	<b>2.14</b>

Table 3: Quantitative results of the MC-CDic model with and without proximal network on IXI testing set.

feature level as 3 in our MC-CDic-L.

**The Effect of the Proximal Network.** In this paper, we employ a proximal network to learn the prior information in a data-driven manner. To validate its effectiveness, we compare the performance of the proposed MC-CDic model with and without the proximal network. Note that when we remove the proximal network, we use the soft-thresholding operator to constrain the learned features. The performance of these two models is shown in Table 3. For the guided-SR task, the proximal network improves the performance by 0.43dB PSNR on the IXI-T2 dataset. For the guided-reconstruction task, the proximal network improves the performance by 1.06dB PSNR on the IXI-T2 dataset. It fully demonstrates the effectiveness of the proposed proximal network.

## 5 Concluding Remarks

We proposed a multi-scale convolutional dictionary model (MC-CDic) for multi-contrast MRI reconstruction and SR. Different from existing DCNN-based methods that manually designed fusion rules to fuse the multi-contrast information, our MC-CDic model was constructed under the guidance of the optimization algorithm with a well-designed data fidelity term. A proximal gradient algorithm was employed to solve the model and the iterative solutions were unfolded into a deep network. Especially, each module in the network could one-to-one correspond to an operation of a solution, thus our model was interpretable. We have tested our MC-CDic model on multi-contrast MRI reconstruction and SR tasks, experimental results demonstrate the superior performance of our method over the existing SOTA methods. In the future, we will explore more applications of our model on multi-modal tasks, such as RGB-guided depth map completion and RGB-guided depth map SR.

## Acknowledgements

This work was supported by the National Key R&D Program of China (2022ZD0161800), the NSFC-RGC (61961160734), the Shanghai Rising-Star Program (21QA1402500), and the Shanghai Municipal Commission of Economy and Informatization Program (2021-GZL-RGZN-01028).

## References

- [Aggarwal *et al.*, 2018] Hemant K Aggarwal, Merry P Mani, and Mathews Jacob. MoDL: Model-based deep learning architecture for inverse problems. *IEEE Transactions on Medical Imaging*, 38(2):394–405, 2018.
- [Beck and Teboulle, 2009] Amir Beck and Marc Teboulle. A fast iterative shrinkage-thresholding algorithm for linear inverse problems. *SIAM Journal on Imaging Sciences*, 2(1):183–202, 2009.
- [Dar *et al.*, 2020] Salman UH Dar, Mahmut Yurt, Mohammad Shahdloo, Muhammed Emrullah Ildız, Berk Tınaz, and Tolga Çukur. Prior-guided image reconstruction for accelerated multi-contrast MRI via generative adversarial networks. *IEEE Journal of Selected Topics in Signal Processing*, 14(6):1072–1087, 2020.
- [Deng and Dragotti, 2020] Xin Deng and Pier Luigi Dragotti. Deep convolutional neural network for multi-modal image restoration and fusion. *IEEE Transactions on Pattern Analysis and Machine Intelligence*, 43(10):3333–3348, 2020.
- [Donoho, 1995] David L Donoho. De-noising by soft-thresholding. *IEEE Transactions on Information Theory*, 41(3):613–627, 1995.
- [Fang *et al.*, 2022] Chaowei Fang, Dingwen Zhang, Liang Wang, Yulun Zhang, Lechao Cheng, and Junwei Han. Cross-modality high-frequency transformer for MR image super-resolution. In *Proceedings of the 30th ACM International Conference on Multimedia*, pages 1584–1592, 2022.
- [Feng *et al.*, 2021] Chun-Mei Feng, Huazhu Fu, Shuhao Yuan, and Yong Xu. Multi-contrast MRI super-resolution via a multi-stage integration network. In *International Conference on Medical Image Computing and Computer-Assisted Intervention*, pages 140–149. Springer, 2021.
- [Feng *et al.*, 2022] Chun-Mei Feng, Yunlu Yan, Geng Chen, Yong Xu, Ying Hu, Ling Shao, and Huazhu Fu. Multi-modal transformer for accelerated MR imaging. *IEEE Transactions on Medical Imaging*, pages 1–1, 2022.
- [Kim *et al.*, 2016] Jiwon Kim, Jung Kwon Lee, and Kyoung Mu Lee. Accurate image super-resolution using very deep convolutional networks. In *Proceedings of the IEEE Conference on Computer Vision and Pattern Recognition*, pages 1646–1654, 2016.
- [Lecouat *et al.*, 2020a] Bruno Lecouat, Jean Ponce, and Julien Mairal. A flexible framework for designing trainable priors with adaptive smoothing and game encoding. *Advances in Neural Information Processing Systems*, 33:15664–15675, 2020.
- [Lecouat *et al.*, 2020b] Bruno Lecouat, Jean Ponce, and Julien Mairal. Fully trainable and interpretable non-local sparse models for image restoration. In *European Conference on Computer Vision*, pages 238–254. Springer, 2020.
- [Li *et al.*, 2022] Guanyuan Li, Jun Lv, Yapeng Tian, Qi Dou, Chengyan Wang, Chenliang Xu, and Jing Qin. Transformer-empowered multi-scale contextual matching and aggregation for multi-contrast MRI super-resolution. In *Proceedings of the IEEE/CVF Conference on Computer Vision and Pattern Recognition*, pages 20636–20645, 2022.
- [Liang *et al.*, 2021] Jingyun Liang, Jiezhong Cao, Guolei Sun, Kai Zhang, Luc Van Gool, and Radu Timofte. SwinIR: Image restoration using swin transformer. In *Proceedings of the IEEE/CVF International Conference on Computer Vision (ICCV) Workshops*, pages 1833–1844, 2021.
- [Liu and Lei, 2021] Cong Liu and Pengcheng Lei. An efficient group skip-connecting network for image super-resolution. *Knowledge-Based Systems*, 222:107017, 2021.
- [Liu *et al.*, 2019] Risheng Liu, Shichao Cheng, Long Ma, Xin Fan, and Zhongxuan Luo. Deep proximal unrolling: Algorithmic framework, convergence analysis and applications. *IEEE Transactions on Image Processing*, 28(10):5013–5026, 2019.
- [Liu *et al.*, 2021] Risheng Liu, Jinyuan Liu, Zhiying Jiang, Xin Fan, and Zhongxuan Luo. A bilevel integrated model with data-driven layer ensemble for multi-modality image fusion. *IEEE Transactions on Image Processing*, 30:1261–1274, 2021.
- [Liu *et al.*, 2022] Tianlin Liu, Anadi Chaman, David Belius, and Ivan Dokmanić. Learning multiscale convolutional dictionaries for image reconstruction. *IEEE Transactions on Computational Imaging*, 8:425–437, 2022.
- [Lu *et al.*, 2021] Liying Lu, Wenbo Li, Xin Tao, Jiangbo Lu, and Jiaya Jia. MASA-SR: Matching acceleration and spatial adaptation for reference-based image super-resolution. In *Proceedings of the IEEE/CVF Conference on Computer Vision and Pattern Recognition*, pages 6368–6377, 2021.
- [Lyu *et al.*, 2020] Qing Lyu, Hongming Shan, Cole Steber, Corbin Helis, Chris Whitlow, Michael Chan, and Ge Wang. Multi-contrast super-resolution MRI through a progressive network. *IEEE Transactions on Medical Imaging*, 39(9):2738–2749, 2020.
- [Menze *et al.*, 2015] Bjoern H. Menze, Andras Jakab, Stefan Bauer, and Kalpathy-Cramer. The multimodal brain tumor image segmentation benchmark (brats). *IEEE Transactions on Medical Imaging*, 34(10):1993–2024, 2015.
- [Nitski *et al.*, 2020] Osvald Nitski, Sayan Nag, Chris McIntosh, and Bo Wang. CDF-Net: Cross-domain fusion network for accelerated MRI reconstruction. In *International Conference on Medical Image Computing and Computer-Assisted Intervention*, pages 421–430. Springer, 2020.
- [Ronneberger *et al.*, 2015] Olaf Ronneberger, Philipp Fischer, and Thomas Brox. U-net: Convolutional networks for biomedical image segmentation. In *International*



- Conference on Medical Image Computing and Computer-Assisted Intervention*, pages 234–241. Springer, 2015.
- [Simon and Elad, 2019] Dror Simon and Michael Elad. Rethinking the CSC model for natural images. *Advances in Neural Information Processing Systems*, 32:2271–2281, 2019.
- [Song *et al.*, 2019a] Pingfan Song, Lior Weizman, João FC Mota, Yonina C Eldar, and Miguel RD Rodrigues. Coupled dictionary learning for multi-contrast MRI reconstruction. *IEEE Transactions on Medical Imaging*, 39(3):621–633, 2019.
- [Song *et al.*, 2019b] Pingfan Song, Lior Weizman, João FC Mota, Yonina C Eldar, and Miguel RD Rodrigues. Coupled dictionary learning for multi-contrast MRI reconstruction. *IEEE Transactions on Medical Imaging*, 39(3):621–633, 2019.
- [Sriram *et al.*, 2020] Anuroop Sriram, Jure Zbontar, Tullie Murrell, Aaron Defazio, C Lawrence Zitnick, Nafissa Yakubova, Florian Knoll, and Patricia Johnson. End-to-end variational networks for accelerated MRI reconstruction. In *International Conference on Medical Image Computing and Computer-Assisted Intervention*, pages 64–73. Springer, 2020.
- [Sun *et al.*, 2019] Liyan Sun, Zhiwen Fan, Xueyang Fu, Yue Huang, Xinghao Ding, and John Paisley. A deep information sharing network for multi-contrast compressed sensing MRI reconstruction. *IEEE Transactions on Image Processing*, 28(12):6141–6153, 2019.
- [Wang *et al.*, 2016] Shanshan Wang, Zhenghang Su, Leslie Ying, Xi Peng, Shun Zhu, Feng Liang, Dagan Feng, and Dong Liang. Accelerating magnetic resonance imaging via deep learning. In *IEEE 13th International Symposium on Biomedical Imaging (ISBI)*, pages 514–517. IEEE, 2016.
- [Wang *et al.*, 2020] Hong Wang, Qi Xie, Qian Zhao, and Deyu Meng. A model-driven deep neural network for single image rain removal. In *Proceedings of the IEEE/CVF Conference on Computer Vision and Pattern Recognition (CVPR)*, pages 3103–3112, June 2020.
- [Wang *et al.*, 2021] Haoqian Wang, Xiaowan Hu, Xiaole Zhao, and Yulun Zhang. Wide weighted attention multi-scale network for accurate MR image super-resolution. *IEEE Transactions on Circuits and Systems for Video Technology*, 32(3):962–975, 2021.
- [Wang *et al.*, 2022] Hong Wang, Yuexiang Li, Deyu Meng, and Yefeng Zheng. Adaptive convolutional dictionary network for CT metal artifact reduction. In *The 31st International Joint Conference on Artificial Intelligence*, pages 1401–1407, 2022.
- [Xiang *et al.*, 2018] Lei Xiang, Yong Chen, Weitang Chang, Yiqiang Zhan, Weili Lin, Qian Wang, and Dinggang Shen. Deep-learning-based multi-modal fusion for fast MR reconstruction. *IEEE Transactions on Biomedical Engineering*, 66(7):2105–2114, 2018.
- [Yang *et al.*, 2018] Yan Yang, Jian Sun, Huibin Li, and Zongben Xu. ADMM-CSNet: A deep learning approach for image compressive sensing. *IEEE Transactions on Pattern Analysis and Machine Intelligence*, 42(3):521–538, 2018.
- [Zamir *et al.*, 2022] Syed Waqas Zamir, Aditya Arora, Salman Khan, Munawar Hayat, Fahad Shahbaz Khan, and Ming-Hsuan Yang. Restormer: Efficient transformer for high-resolution image restoration. In *Proceedings of the IEEE/CVF Conference on Computer Vision and Pattern Recognition*, pages 5728–5739, 2022.
- [Zhang *et al.*, 2018] Yulun Zhang, Kunpeng Li, Kai Li, Lichen Wang, Bineng Zhong, and Yun Fu. Image super-resolution using very deep residual channel attention networks. In *Proceedings of the European conference on computer vision (ECCV)*, pages 286–301, 2018.
- [Zhang *et al.*, 2021a] Jinwei Zhang, Hang Zhang, Chao Li, Pascal Spincemaille, Mert Sabuncu, Thanh D Nguyen, and Yi Wang. Temporal feature fusion with sampling pattern optimization for multi-echo gradient echo acquisition and image reconstruction. In *International Conference on Medical Image Computing and Computer-Assisted Intervention*, pages 232–242. Springer, 2021.
- [Zhang *et al.*, 2021b] Yulun Zhang, Kai Li, Kunpeng Li, and Yun Fu. MR image super-resolution with squeeze and excitation reasoning attention network. In *Proceedings of the IEEE/CVF Conference on Computer Vision and Pattern Recognition*, pages 13425–13434, 2021.
- [Zhao *et al.*, 2019] Xiaole Zhao, Yulun Zhang, Tao Zhang, and Xueming Zou. Channel splitting network for single MR image super-resolution. *IEEE Transactions on Image Processing*, 28(11):5649–5662, 2019.
- [Zheng *et al.*, 2019] Hao Zheng, Faming Fang, and Guixu Zhang. Cascaded dilated dense network with two-step data consistency for MRI reconstruction. *Advances in Neural Information Processing Systems*, 32:1742–1752, 2019.